Physicochemical, mechanical, barrier and antibacterial properties of starch nanocomposites crosslinked with pre-oxidised sucrose

Preetha Balakrishnan[a], Sreekala M.S.[b], Geethamma V.G.[a], Nandakumar Kalarikkal[a], Vanja Kokol[c], Tatiana Volova[d], Sabu Thomas[a,d,e,]

[a]International and Inter University Center for Nanoscience and Nanotechnology, PD Hills P.O, Mahatma Gandhi University, Kottayam, Kerala 686560, India
[b]Department of Chemistry, Sree Sankara College Kalady, Ernakulum, Kerala, 683574, India
[c]Institute for Engineering Materials and Design, University of Maribor, Smetanova ul. 17, 2000 Maribor, Slovenia
[d]Siberian Federal University, 79 Svobodnyi Av., Krasnoyarsk, 660041, Russia
[e]School of Chemical Sciences, Mahatma Gandhi University, PD Hills P.O, Kottayam, Kerala 686560, India

Keywords: Biopolymer, Oxygen permeability, Water vapor transmission rate, Modelling Packaging

A B S T R A C T

Bionanocomposite films were fabricated using starch as a matrix, pre-oxidised sucrose as a crosslinker and cellulose nanofibres as reinforcement filler. The spectroscopic (FTIR) and microscopic (SEM) techniques were used to identify the chemical changes associated with the crosslinking, and to characterize the morphological structure of the films. The crosslinking density evaluated by Flory-Rehnar equation. There is a decrease in diff usivity, permittivity and swelling properties of the films after crosslinking. Reduction of water vapour (from 0.074 to 0.038 g min−1 m^{-2}) and oxygen (from 29.44 to 10.27 cm^3 m^{-2} d^{-1}) transmission rates for film prepared with 3 wt.% of OS and 5 wt.% of CNFs was observed. The water transport through the films was found to follow Fickian behaviour. The antibacterial properties of films against four diff erent food pathogens were evaluated. Films represent high potential alternative to existing ones.

1. Introduction

Bio-based materials have gained much attention in recent years due to the depletion, environmental and health issues associated with petroleum-based materials (Matzinos et al., 2002). However, most of the packaging material based on biopolymers faces the drawback of poor mechanical and barrier properties. Excessive studies have been thus conducted to reduce the water sensitivity of biopolymer composites, which include blending, crosslinking and chemical modifications (Staroszczyk et al., 2017; Li

et al., 2018; Luchese et al., 2017; Zhang et al., 2017).

Starch is a semi-crystalline polymer abundantly available in nature as tubers, pulses, cererals etc. Starch is a polymeric carbohydrate consisting of large number of glucose units joined by glycosidic bonds (Teacă et al., 2013). Native starch is, typically, very brittle, and not easy to process due to the strong inter and intra molecular hydrogen bonding interaction between the adjacent groups. In order to make it more flexible, non-volatile and small molecule plasticizers like sorbitol, (Mathew and Dufresne, 2002) glycerol, (Balakrishnan et al., 2017) urea (Tang et al., 2008) etc were used. Plasticizers improves the flexibility of films by reducing the brittleness (Liu et al., 2009). Because of the amorphous region (formed by amylose and branching units of amylo- pection) starch has low mechanical properties. This can be elevated by incorporating nanoinclusion like cellulose, clay, chitin etc. Cellulose, the building material of long fibrous cells, is a strong natural polymer. Cellulose based materials from various biological sources (leaf, wood, cotton etc.) has been used for varying applications. Cellulose nanofibers are intrinsically low cost and are readily available. Thus, cellulose na- nofiber based composites are an attractive class of nanomaterials on account of low cost, lightweight and high-strength.

Modification of starch based material is carried out to reduce the shortcoming of pristine starch to increase its versalility. The blending with synthetic polymers such as polycaprolactone, (Averous et al., 2000) polyethylene, (Da Róz et al., 2012) poly lactic acid (Akrami et al., 2016) etc., improves the final performance of starch based materials. Starch modification can be primarily classified as five categories; physical, chemical, grafting, enzymatic and crosslinking (Kim et al., 2017; Teacă et al., 2013). Crosslinking is one of the method to improve the properties of starch films, although it is usually associated with physical and chemical incompatibility between the two polymers. Crosslinking initiates formation of bridges between adjacent molecules by using diff erent crosslinking agents (Veiga-Santos et al., 2007; Xie et al., 2014; Dang and Yoksan, 2016). Starch and starch based products have been crosslinked with diff erent crosslinkers were earlier reported, such as sodium trimetaphosphate (Chen et al., 2017), urea formaldehye(Mittal et al., 2016), epichlorohydrin (Zhou et al., 2016). However, most of them are toxic, or even carcinogenic (Laskin et al., 1980), and many of them are relative expensive (Yin et al., 2005). Incorporating citric acid as a crosslinker substantially reduced the tensile stress of the products developed under the conditions used (Reddy and Yang, 2010). How- ever, the chemicals used for crosslinking starch are relatively toxic, expensive or do not provide the desired improvement in properties. Highly reactive aldehyde derivatives showed satisfactory mechanical performance and stability (Xu et al., 2015).

Antimicrobial packaging has been used for the inhibition of certain bacteria in foods, but barriers to their commercial implementation continue to exist (Assis et al., 2017). Antimicrobial packaging is an area with high potential for applying bio-nanocomposite technology to control undesirable microorganisms on foods by means of the in- corporation of active molecules such as antimicrobial compounds in or coated

onto the packaging materials (Abdel-Halim and Al-Deyab, 2014; Xu et al., 2013).

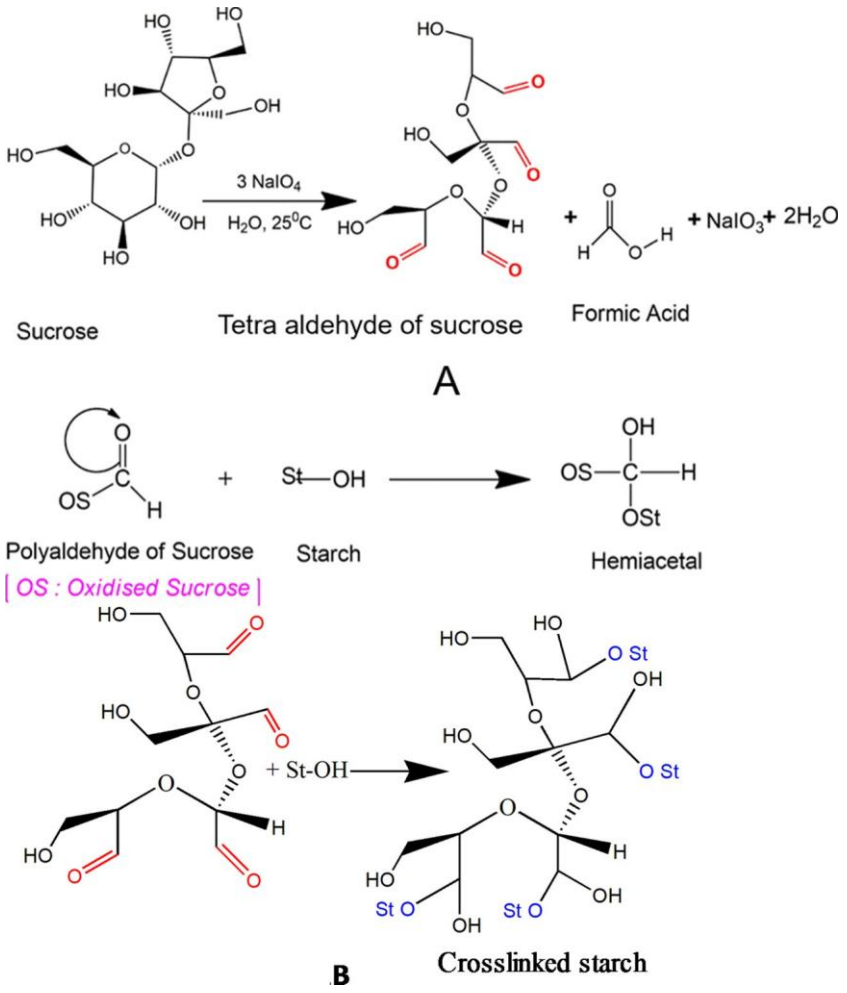

Scheme 1. Possible reaction mechanism between starch and oxidised sucrose.

Sucrose is disaccharides which can be modified into its aldehyde derivative by periodate treatment. Periodate reaction selectively oxidase's the vicinal hydroxyl groups in sucrose to aldehyde derivative. Neter et al. (1956) studies the eff ect of periodate oxidation on the polysaccharides. They found that oxidation of the *Escherichia coli* lipo polysaccharide with periodate yields a compound of low toxicity and marked pyrogenicity (NETER et al., 1956). Starch nanocomposites modified with cellulose nanofibrils and nanocrystals have been reported (Balakrishnan et al., 2017; Das et al., 2011; Liu et al., 2010; Prachayawarakorn et al., 2010), herein we propose the eff ect of a biocrosslinker and cellulose nanomaterial on the mechanical, barrier and antibacterial properties of starch based films. In this work, cross- linking of starch with a non-toxic disaccharide, i.e. a derivative sucrose aldehyde, and its further reinforcement with cellulose nanofibrils (CNFs), was studied to obtain bio-based composite films with a good mechanical strength, high flexibility and barrier properties to be used for food

packaging applications.

2. Materials and methods

2.1. Materials

For the preparation of plasticized starch (PS) corn starch (containing approx. 73% of amylopectin and 27% of amylose) and glycerol ($C_3H_8O_3$, molar weight of 92.09 g mol^{-1}) were used sucrose (average molar weight of 342.49 g mol^{-1}), sodium periodate and potassium chloride were purchased from Sigma Aldrich and used without any further purification. Cellulose nanofibrils (CNFs) of about 20-50 nm in diameter and up to several μm in lenght was obtained from pineapple leaf fiber as we reported earlier (Balakrishnan et al., 2017). Shortly, dried pineapple leaf first chopped and milled to fine powder and subjected to alkaline treatment using 2% NaOH in an autoclave kept under pressure of 138 kPa for 1 h, after that pressure released immediately. The alkali treated fiber then bleached using equal parts of NaOH and glacial acetic acid (27 g/L and 78.5 g/L respectively) for 30 min. The white residue after bleaching were treated with 11% oxalic acid in an autoclave set at 138 kPa for 15 min and centrifuged.

2.2. Oxidation of sucrose

The oxidised sucrose (OS) was obtained via periodate cleavage, using the procedure adapted from Xu et al. (Xu et al., 2015) with minor modifications. For oxidation reaction, 10 g of sucrose was mixed with 15 g of sodium periodate in 300 ml distilled water. The solution was stirred for 24 h at room temperature before 7 g of potassium chloride was added, followed by stirring for another hour at 5 °C until complete precipitation. The solution was then filtered with cheese cloth to obtain the liquid, which was a polyaldehyde of sucrose. The oxidised sucrose of around 7 wt.% and pH 2.5 was stored in a refrigerator for further use. The low pH of the solution was due to the existence of formic acid as a by-product from the oxidation (Canisag, 2015), as shown in Scheme 1.

2.3. Fabrication of the films

For the reference film, 10 g of starch was mixed with 30 wt. % of glycerol, based on the dry weight of starch, and dispersed in 100 ml distilled water by heating at 90 °C and stirring with a magnetic stirrer for 30 min. The resulting viscous suspension was poured into levelled petri dishes and kept at room temperature for about 72 h (Balakrishnan et al., 2017) to get them fully dried. Crosslinked films were prepared by varying concentrations of oxidised sucrose such as 1, 2, and 3 wt. % where M_c is the molecular weight of polymer between crosslinks, ρ_r is the density of the polymer, V_s and

V_{rf} are the molar volume of the solvent and volume fraction of the polymer in the swollen sample respectively, *d* represents deswollen weight, *f* is the volume fraction of filler, *w* is the initial weight of the material, and A_s is the amount of solvent adsorbed by the material. The interaction parameter χ, shown in Eq. (4), is given by the Hildebrand equation:(based on the dry weight of starch) (PS + OS1, PS + OS2, PS + OS3 respectively). The same procedure was used to prepare crosslinked $\chi = \beta + [V_s(\rho_s - \rho_p)^2/RT$](6) nanocomposite films with the addition of 1, 3, and 5 wt.% of CNF dispersions. The films were dried in an oven at 70 °C for 24 hs to allow complete crosslinking.

2.4. Determination of aldehyde groups` (CHO) content

The aldehyde content of the OS was analysed by the volumetric titration method. Dried oxidised substrate (0.2 g) was weighed into a 125 mL conical flask, and 10 mL of standardised 0.2 M sodium hydroxide was added. The flask was swirled in a water bath at 70 ± 2 °C for 2 min, then cooled immediately under running tap water with rapid swirling for 1 min. 10 mL of standardised 0.2 M sulfuric acid, 50 mL of water and 1 mL of 0.2% phenolphthalein was added in turn. The titration of the acid solution was carried out using 0.2 M sodium hydroxide (Hofreiter et al., 1955; Zhang et al., 2014) and the percentage of aldehyde content was calculated by using the following equation:

$$\mathrm{CHO}\,\% = \frac{V_1 C_1 - 2V_2 C_2}{(W/161) \times 1000} \times 100\% \quad (1)$$

where, C1and C2 are normality of NaOH and H2SO4 in (mol/L), respectively, V1 and V2 are total volume of NaOH and H2SO4 (mL), respectively, W is the dry weight of the OS, and 161 is the average molecular weight of repeating units of OS. The experiments were done in triplicate

2.5. Fourier transform infrared spectroscopy (FTIR) analysis

FTIR analysis was performed by a Perkin-Elmer spectrometer with a golden gate ATR accessory attached to a diamond crystal. The spectra were recorded in ambient condition from average of 16 scans at the resolution of 4 cm−1 within the region of 4000–100 cm^{-1}. Before the analysis, the samples were conditioned at 50 ± 2 °C for 45 min, to ensure no moisture adherence to the sample.

2.6. Evaluation of the film's swelling and crosslinking density

The film samples were cut into circular specimens of 2 cm diameter to be

analysed for water absorption according to the gravimetrical method using Standard ASTM D5890 and a highly sensitive electronic balance. To evaluate the effect of drying on water sorption, two sets of samples were used for the study: one without the drying and the other after drying at 70 ± 2 °C for 24 h. The percentage of increase in swollen mass was calculated by the following equation:

$$\text{Swollen mass increase (\%)} = [(m_1 - m_0)/m_0] \times 100 \quad (2)$$

where m_0 is the initial weight of the sample and m1 is the weight of the sample after immersing into the solvent milliQ water in which the solvent specimens were cleared by using filter paper. The density of the crosslinking is then calculated from the equilibrium swelling data by means of the Flory-Rehner equations (John et al., 2008; Saleesung et al., 2017; Xu et al., 2017):

$$V = 1/2\, M_c \quad (3)$$

$$M_c = [-\rho_r\, V_s\, V_{rf}^{1/3}]/[\ln(1 - V_{rf}) + V_{rf} + \chi V_{rf}^2] \quad (4)$$

$$V_{rf} = [(d - fw)\rho_r]/[([(d - fw)\rho_r]) + (A_s/\rho_s)] \quad (5)$$

where Mc is the molecular weight of polymer between crosslinks, ρ_r is the density of the polymer, V_s and V_{rf} are the molar volume of the solvent and volume fraction of the polymer in the swollen sample respectively, d represents deswollen weight, f is the volume fraction of filler, w is the initial weight of the material, and As is the amount of solvent adsorbed by the material. The interaction parameter χ, shown in Eq. (4), is given by the Hildebrand equation:

$$\chi = \beta + [V_s(\rho_s - \rho_\rho)^2/RT] \quad (6)$$

where β is the lattice constant, R represents the universal gas constant, T is the absolute temperature, ρs and ρρ are the solubility parameters of solvent and polymer respectively.

2.7. Scanning Electron Microscopy (SEM) analysis

SEM images of the films were performed with an Ultra + (Zeiss, Germany) microscope to analyse the surface morphology of the films. For this purpose, the samples were cryo-fractured in liquid nitrogen. The samples were coated with a thin platinum layer using a sputter PECS-Precision coating system, model 682 (Gatan US).

2.8. Water contact angle measurement

Contact angle measurements of the films using milli Q water were performed

using an SCA 20 Contact Angle measurement system from Dataphysics (Germany). Each contact angle value was an average value of six measurements.

2.9. Moisture sorption

The moisture sorption of prepared films was analysed by ASTM d570 in a climate chamber at a relative humidity (RH) of 75 ± 5%. Samples were cut into 30 mm × 10 mm rectangular strips. Prior to the analysis, the samples were vacuum dried at 50 ± 2 °C overnight. The samples were taken out from the climate chamber at predetermined intervals and gain in weight was analysed with a precision of 0.01 g. Triplicates of each samples were taken. The percentage of moisture absorption was analysed using the following equation:

$$\text{Moisture sorption } (\%) = \frac{m_{f-m_i}}{m_i} \times 100 \quad (7)$$

where, m_f and m_i are final and initial weight of samples, respectively.

2.10. Diff usion experiment

Circular specimens of 2 cm diameter were cut using a sharp-edged dye. The samples were then immersed in a beaker containing distilled water. The samples were removed at regular intervals and weighed immediately in an electronic balance. The samples were wiped gently with a soft tissue before weighing to avoid moisture adhering into the sample. Triplicates of each samples were taken.

2.11. Water vapour transmission rate (WVTR) determination

The WVTR of the films was determined according to the ASTM E96-95 Standard (Desiccant method). The films were cut into a circle of 6.3 cm diameter and sealed onto an aluminum permeation cup containing 45 g of dry calcium chloride with silicone grease, and a ring was used to hold the films in place. The whole device was weighed and then placed in a climatically controlled chamber (32° ± 2 °C and 50 ± 5% RH). The prepared films were sealed into the permeation cup and weighed at regular time intervals, and a linear relationship was obtained between the quantity of water transferred per unit of air and time. WVTR for three specimens of each sample was calculated as shown by the equation.

$$\text{WVTR} = \frac{m_2 - m_1}{1440 * r^2} \, (g \, min^{-1} \, m^{-2}) \quad (8)$$

where m_2 and m_1 are final and initial weight respectively, and r is the radius of the permeation cup.

2.12. Oxygen transmission rate (OTR) determination

The samples were conditioned at a temperature of 23 ± 2 °C and 50 ± 5% RH 24 h before measuring the OTR. OTR was determined at the same conditions using a Perme OX2/230 (Labthink Instruments Co.,Ltd.). Film thickness was measured with an electronic digital caliper before testing and input to the computer programme WinPerme OX2-230 W3-330(En). The OTR was measured after the film had been placed in a cell, and the oxygen flow introduced on one side of the film. The OTR (ml m^{-2} day^{-1}) was calculated from the mean OTR multiplied by the film thickness (mm) and divided by the oxygen gradient within the cell of the testing machine (1 kgf cm−2). Three independent determinations were carried out for each film sample, and the mean of those three values is given as the final result.

2.13. Mechanical properties testing

Tensile properties of the films were evaluated by a smit weld tensile test unit in accordance with the ASTM 638 Standard. The tensile test was carried out at room temperature with a crosshead speed of 10 mm/min and load cell of 500 N. Triplicates of each samples were carried out.

2.14. Anti-bacterial studies

2.14.1. Bacteria and growth conditions

Four bacterial species were employed as test organisms which include Staphylococcus aureus, Escherichia coli, Salmonella typhimurium, Bacillus cereus. The bacteria were maintained in Mueller-Hinton Agar (MH). Inocula were prepared by adding an overnight culture of the organism in MH broth to obtain an OD600 0.1. The cells were allowed to grow until they obtain the McFarland standard 0.5 (approximately 108CFU/ml). The suspension were then diluted 1:100 in MH broth to obtain 106CFU/ml.

2.14.2. Test products

2.14.2.1. Determination of antibacterial activity. These discs were placed on Mueller-Hinton agar plates, previously swabbed with the targetacterial isolate at a concentration of 106 CFU/ml. Inone disc, the respective organic solvent was added as negative control to determine possible inhibitory activity of the solvent. This preparation was incubated for a period of 24 h at 30 °C. Antibacterial activity was defined as the diameter (mm) of the clear inhibitory zone formed around the discs. The Minimum inhibitory concentration (MIC) of the extract was determined by tube dilution techniques in Mueller-Hinton broth (Merck) according to national committee for clinical laboratory standards (NCCLS). Minimum inhibitory concentration (MIC) is the lowest concentration of a chemical which prevents visible growth of a bacterium. The range of

concentration used was 156.25 to 5000 μg/ml. The four last vials of each bacterium with no growth from the MIC procedure were streaked onto nutrient agar (NA) plates.

3. Results and discussion

3.1. Oxidation of sucrose and its crosslinking with the starch and CNF

Sucrose is a non-reducing disaccharide sugar that has to be oxidised first by a suitable oxidant to convert its hydroxyl groups into carbonyl functionalities (mainly aldehydes, CHO and ketones, C=O) to obtain polyaldehyde derivative, which would be then used to crosslink the starch polymers, as well as CNFs. In the presence of sodium periodate, the vicinal hydroxyl groups of sucrose are, thus, cleaved to form a tetra aldehyde derivative of sucrose with high yield (Mithra and Perlin,1959), following the reaction mechanism presented in Scheme 1A. During the reaction, the formic acid is produced as a by-product and, as a result, the resulting product has pH of ˜2–3. The aldehyde groups in the oxidised sample were express as the number of carbonyl group per 100 glucose units. The percentage of aldehydes formed was calculated volumetrically by the titration method, and it was found to be around 30 ± 5% per molecule of sucrose calculated by volumetric titration method.

3.2. Structural properties of films

The FTIR spectroscopy was used to analyse the oxidation of the sucrose, as well as its crosslinking with the starch polymers and CNFs during the film preparation. The aldehyde (C=O) groups of OS shall react with the hydroxyl (O–H) groups of starches (PS) to form ether bonds (C–O–C) as presented in Scheme 1B.

As shown on Fig. 1A, the spectra of both native and OS had a characteristic broad peak at about 3000-3500 cm^{-1} which corresponds to the hydroxyl (O-H) stretching vibration, and a duplet peak between 2820 and 3000 cm^{-1} due to the C-H stretching related to aldehydes and the alkyl chain, respectively. The absorbance intensitiy at 3200-3500 cm^{-1} band in the spectrum of OS sample is much lower and broaden, indicating a strong interaction of sucrose hydroxyl groups with the periodate and resulting in the decrease in the amount of hydroxyl groups by their conversion into aldehyde derivatives (Kumirska et al., 2010), which can be seen by a new peak appeared at about1646 cm^{-1} for OS sample, corresponding to the conjugated stretching vibration of the aldehyde (C=O) groups.

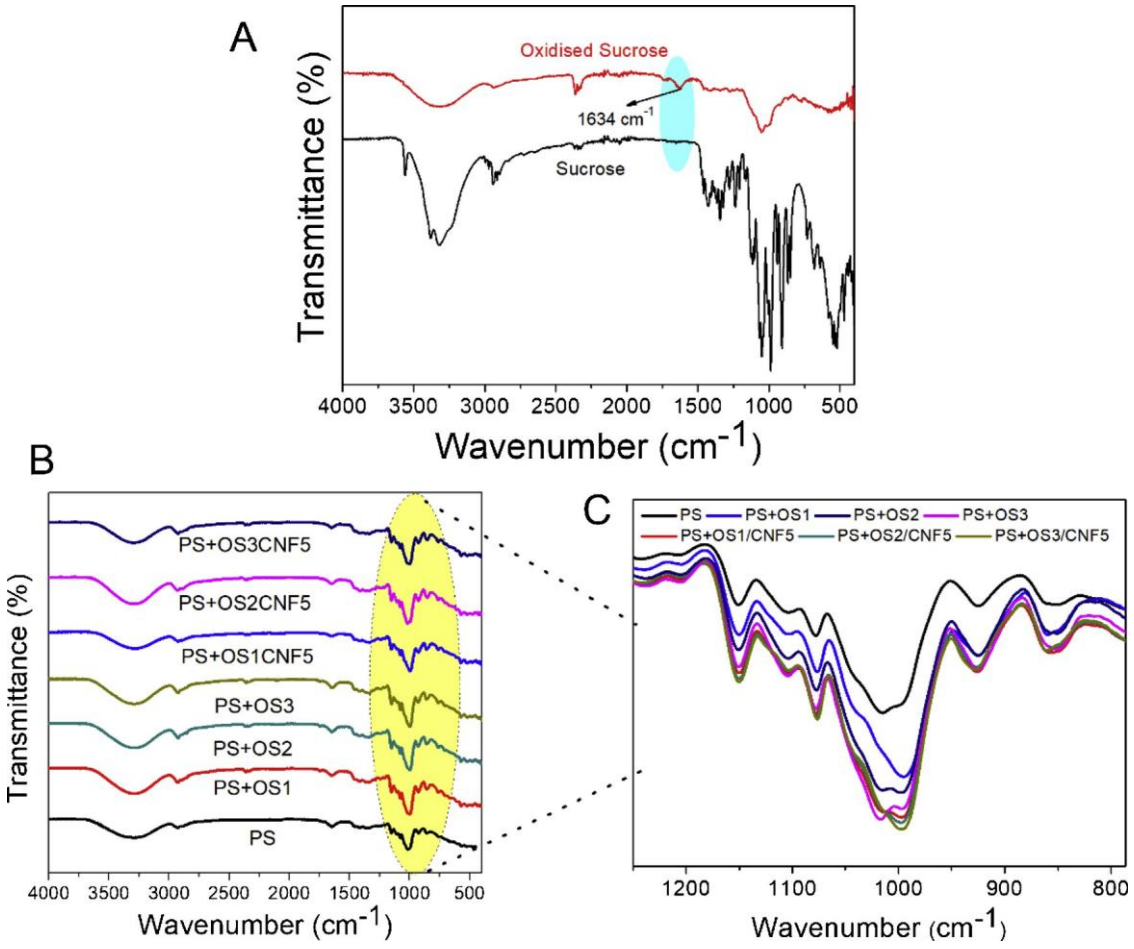

Fig. 1. FTIR spectra of (A) sucrose and oxidised sucrose (OS) and (B) uncross linked and crosslinked nanocomposite films with magnified image in the range (C) of 1200-800 cm^{-1} corresponding to the ether/acetal (CeO) stretching.

The FTIR spectra of starch films with and without of OS and CNFs, respectively, are shown in Fig. 1B. All spectra were further magnified in the region between 1200-800 cm^{-1} (Fig. 1C) assigned to the C-O stretching vibrations of primary, secondary and tertiary alcohols (being seen by three small peak's between 1200-1050 cm^{-1}) and β-(1→4)-glycosidic linkages (a broad band with two peaks centered at around 1000 cm^{-1}) of both starch and CNF. It can be seen from the spectra of films prepared with OS only, that the peaks for C-O stretching vibrations between 1200-1050 cm^{-1} are getting larger by OS content in- creasing, resulting from the formation of the ether linkages upon re- action of the PS with the OS. In the spectrum of PS + OS3, these peaks became the largest due to the highest crosslinking level and the formation of more ether linkages. At the same time the absorbance intensity ratio of bands for O-H and C-H relatively decreased, while the band at about 1640 cm^{-1} is overlapping with the larger band at about 1650 cm^{-1} corresponds to C=C bond. By the addition of CNF, the C-O stretching vibrations band between 1200-1050 cm^{-1} are further intensified a bit, indicating that the OS may form ester linkages also with hydroxyl groups of CNF.

Overall, the ATR-FTIR results indicate that the PS + OS/CNF composites were

partially or highly crosslinked based on the decreased intensity of bands for OeH stretching vibration combined with the in- creased intensity of bands for CeO stretching vibration. The crosslinking reactions can occur between aldehyde groups of OS and hydroxyl groups of the PS as well the CNFs. These results also confirm that a crosslinking, however, was mainly achieved between PS and OS, which mainly because the OS molecules can easily interact with the flexible PS compared to more rigid and semi-crystalline CNF.

The crosslinking densities (υ_c) of the films were calculated using the Flory-Rehnar equation, and are plotted against the molecular weight percent of OS. As shown in the Fig. 2, the crosslink densities increases with the OS concentration from 4.65×10^{4} mol cm^{-3} for 1 wt.% OS to 9.46×10^{4} mol cm^{-3} to 3 wt.% of OS. As shown in Scheme 1, the two-reactive functional groups react with each other, yielding an increase of the molecular weight between the crosslinks (M_c).

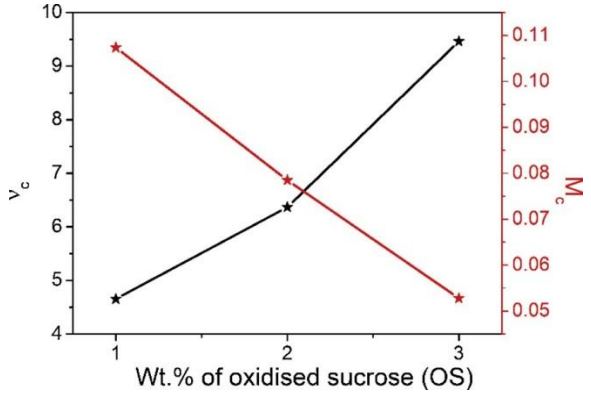

Fig. 2. Crosslinking density (υ_c) and molecular weight between the crosslink (M_c) of the crosslinked starch films prepared with diff erent weight percentages of OS.

3.3. Morphological characteristics

SEM images of diff erently prepared film surfaces are shown in Fig. 3. The fracture surfaces of films prepared with 1 and 3 wt.% of OS (images a and c) indicate a good blending of the OS with the starch, which is becoming highly oriented in the presence of CNFs (images b and d). However, by looking closely into the images, it can be noticed that films crosslinked films showed a rather rough surface, and that the sample with higher OS content. In the case of films prepared with 5 wt.

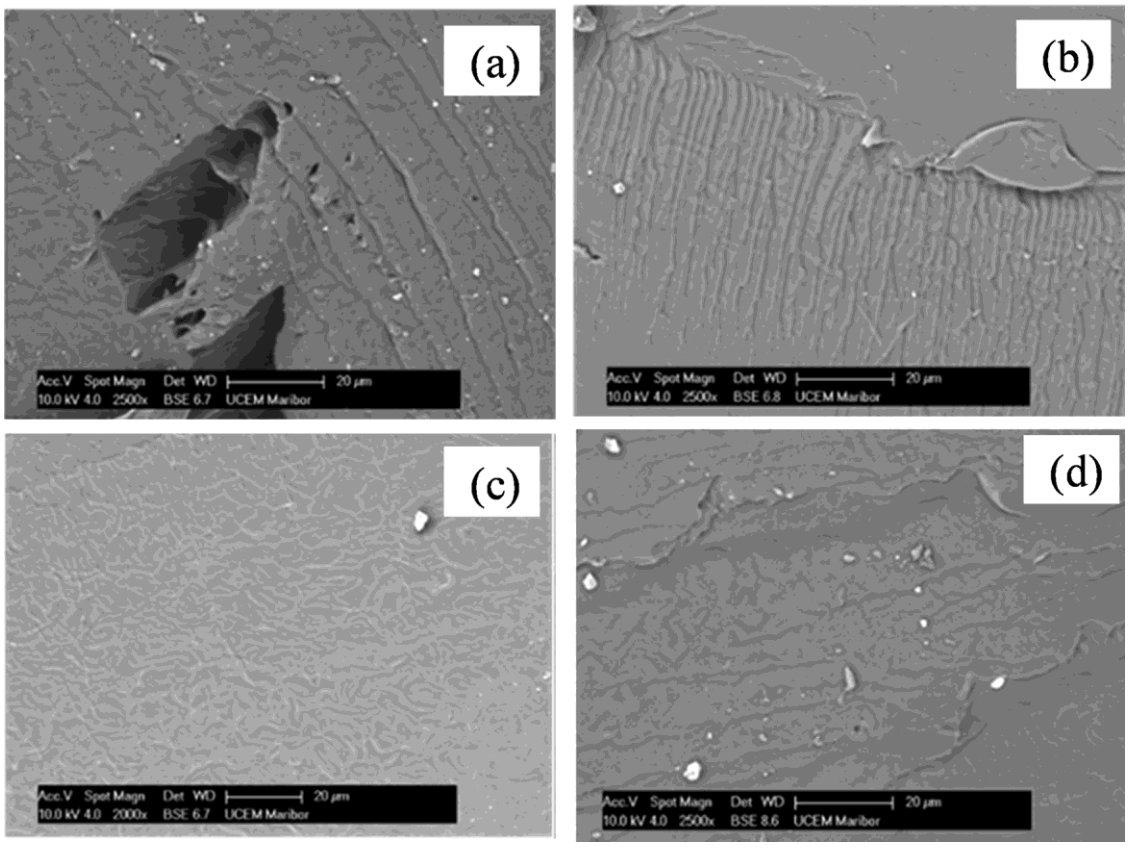

Fig. 3. SEM images of prepared films: (a) PS + OS1, (b) PS + OS1/CNF5, (c) PS + OS3, and (d) PS + OS3/CNF5.

% of CNFs, the fracture surface showed a continuous vein-like (roughen) pattern, indicating an eff ective dispersion of CNFs within the starch polymers, which helps the eff ective stress transfer of load to the matrix. The white spots in the images are because of the presence of unreated crosslinker. However, the images showed no voids and dis- continuity in the matrix and filler interface, indicating on a good adhesion of CNFs with the starch (Rico et al., 2016). The composite sur- face consists of a well-defined vein-like pattern, usually seen when the deformation of the crosslinked samples was controlled by its amorphous homogenous matrix (Garcia et al., 2009).

3.4. Functional properties of the films

As presented in Scheme 1, the hydroxyl groups in the starch react with the aldehyde group in the OS forming acetal linkages, which are much less hydrophilic than hydroxyl groups. The addition of CNFs, which are also a polysaccharide and can easily react in the same way, thus forming a network over the starch polymer chain, thereby creating a tortuous path for the water molecules to enter into the samples (Hietala et al., 2013; Wang et al., 2012). For a deeper understanding, diff erent analytical techniques were applied to get more information about films` hydrophilicity, water and water-vapour sorption, and transportation parameters. These aspects are

important for materials being used in food packaging applications.

Water contact angle measurements were performed to evaluate the hydrophobicity of the films depending on the film composition (Table 1). The treatment produces an increase in the hydrophobic character, which might be due to the lowering of hydroxyl groups in the crosslinked sample by the reaction of starch and OS. Neat starch film prepared without OS shows the lowest contact angle (˜33°), which is due to the presence of a large number of hydroxyl groups from the starch. For the films prepared with OS, the contact angle rises from ˜54° via ˜73° to ˜92° for 1, 2, and 3 wt. % of its addition, respectively, indicating an increased tendency of the film surface hydrophobicity. During drying of the film preparation process, the aldehyde groups in the OS sample enter into reaction with the hydroxyl groups of starch and form water stable acetal linkages, as already discussed and shown in Scheme 1. This reduces the availability of hydroxyl groups gradually and, thereby, increases the contact angle. The addition of CNFs in- creases the contact angle further, thus reaching a value of ˜99° in case of the highest percentage of OS and CNF content.

Table 1
Functional properties of the films.

Sample	Contact angle (θ)	Moisture Sorption (%)	Swelling in water(%)	
			Swelling % (before drying)	Swelling % (after drying at 70 °C)
Neat PS	33.81 ± 2.67	12.36 ± 0.70	14.69 ± 0.13	14.69 ± 0.13
PS + OS1	54.25 ± 0.48	7.53 ± 0.14	7.7 ± 0.08	3.43 ± 0.04
PS + OS1/CNF 1	55.58 ± 0.11	7.21 ± 0.04	6.58 ± 0.23	3.35 ± 0.02
PS + OS1/CNF 3	60.48 ± 0.02	6.55 ± 0.07	6.58 ± 0.09	3.021 ± 0.04
PS + OS1/CNF 5	64.75 ± 0.03	6.44 ± 0.07	7.76 ± 0.05	3.007 ± 0.05
PS + OS2	73.12 ± 0.33	4.59 ± 0.02	7.58 ± 0.03	3.004 ± 0.17
PS + OS2/CNF 1	74.56 ± 0.05	4.56 ± 0.04	6.89 ± 0.10	2.96 ± 0.40
PS + OS2/CNF 3	82.13 ± 0.06	4.37 ± 0.007	6.89 ± 0.14	2.85 ± 0.03
PS + OS2/CNF 5	83.55 ± 0.04	4.29 ± 0.021	6.28 ± 0.02	2.75 ± 0.05
PS + OS3	92.88 ± 0.285	3.92 ± 0.014	6.23 ± 0.02	2.56 ± 0.03
PS + OS3/CNF 1	93.75 ± 0.065	3.68 ± 0.091	5.36 ± 0.04	2.05 ± 0.03
PS + OS3/CNF 3	94.77 ± 0.25	3.35 ± 0.049	5.15 ± 0.09	1.68 ± 0.03
PS + OS3/CNF 5	99.83 ± 0.1	3.25 ± 0.1414	5.06 ± 0.02	1.589

Table 2
Analysis of sorption data of the films.

Sample	n	Diff usion coeffi cient ($x10^5$ cm^2/sec)	Sorption coeffi cient	Permeability coeffi cient ($x10^5$ cm^2/sec)	Swelling coeffi cient	Swelling index (%)
PS	0.43	2.06	5.36	11.04	0.94	96.05
PS + OS1	0.56	1.55	3.54	5.48	0.54	80.03
PS + OS2	0.53	1.13	2.14	2.41	0.43	68.01
PS + OS3	0.54	0.05	2.06	0.10	0.39	45.71
PS + OS1/CNF5	0.58	0.02	1.52	0.03	0.35	38.36
PS + OS3/CNF5	0.53	0.006	1.02	0.006	0.21	19.26

The swelling experiments were conducted to evaluate the eff ect of the crosslinking. As the crosslinking of the films by acetal linkage is highly dependent on the removal of the water molecules, two sets of films were prepared and evaluated: one before and one after their drying at 70 °C. It may be seen from Table 2 that the curing reduces the swelling properties of the samples substantially, indicating that the acetal linking has high influence on the swelling behaviour of the films, acting as a barrier that prevents water molecules from being sur- rounded causing the swelling of the starch granules. The swelling thus reduces substantially for the films prepared with the OS (from ˜14.69% to ˜1.5%) and further with the addition of CNFs (from ˜3.3% to ˜1.5%), compared to the reference starch sample (˜14.7).

Starch has very low moisture resistance due to its hydrophilic nature (Arun et al., 2012), thus the moisture sorption of diff erently prepared films was studied at a relative humidity of 50% and room temperature. As seen from Table 1, the moisture sorption values reduces gradually from the reference sample (˜12.3%) to the films prepared with OS (from ˜7.5% to ˜3.9%), as well as CNFs (from ˜7.2% to ˜3.2%), depending on their concentration used. The acetal linkage between the hydroxyl groups of starch/CNFs and aldehyde groups of the OS reduces the hydrophilic hydroxyl groups substantially, thus stabilising the starch matrix phase when subjected to the moisture atmosphere. This leads to a preferential penetrant path, and to a detrimental eff ect on barrier properties (García et al., 2009; Kaushik et al., 2010). Similar trends were also reported by other authors (Mathew and Dufresne, 2002; Mathew and Dufresne, 2002). Further decrease of moisture sorption with the CNFs` presence can be due primarily to the formation of a more dense network which hinders the segmental mobility of polymer chains, forming a network over the polymer chain and, thereby, creates a tortuous path for the water molecules to enter into the samples (Karim et al., 2014; Kaushik et al., 2010; Hietala et al., 2013; Wang et al., 2012).

3.5. Transport properties

Transport of solvents through the polymer framework relies upon a few parameters, similar to free volume of network starch, the penetrant size of molecule, crosslink densities, level of fortification, and so forth. Diff usion of solvent/water (Q_t)

molecules through the samples was calculated using the following equation:

$$Qt \ \ mol\% = \frac{(Mass\ of\ sovent\ \ absorbed\ /\ Molarmass\ of\ \ solvent)}{Mass\ of\ \ polymer} \times 100 \tag{9}$$

and a graph Qt vs. T1/2 was plotted. It can be seen from the Fig. 4 that the molar uptake of water increases very rapidly in the PS because of its high hygroscopic nature, and is being reduced kinetically and quantitatively at the OS crosslinked samples (PS+OS), leading to a considerable sorption reduction due to an effective crosslinking of OS with the starch. It can also be observed that the swelling continues at a considerably fast rate, since the concentration gradient of penetrate solvent molecules is larger in the matrix. The least solvent absorption was recorded for PS+OS3/CNF5, which is due to the synergistic effect of the crosslinker, as well as well dispersed reinforcing filler CNFs in the matrix phase, by which polymer chain mobility is becoming restricted and reduced free volume, resulting in a reduced solvent absorption and diff usion through the matrix (Abraham et al., 2015). The equilibrium of solvent absorption is, thus, reduced considerably in the crosslinked and CNFs reinforced films (PS + OS1/CNF5 and PS + OS3/CNF5).

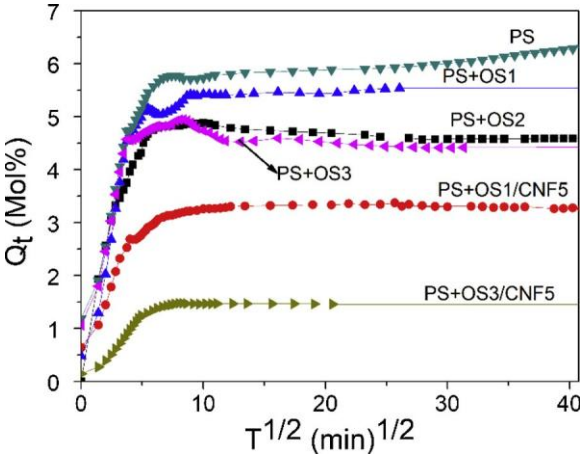

Fig. 4. Sorption curve of the nanocomposite films.

The transport mechanism and behaviour of solvent penetration can be understood better by using the following formula (Abraham et al., 2015)

$$\log Q_t/Q_\infty = \log k + n \log t \tag{10}$$

where Q_t is the mole percent of solvent uptake, k is a constant that depends on the structural characteristics of polymer and solvent interaction, and n is the mode of

sorption mechanism. The values n and k were determined by taking the power regression analysis of linear portion of Q_t vs. $T^{1/2}$ graph (Fig. 4). The value of n determines the sorption mechanism. If $n = 0.5$, the mode of transport is Fickian, in which the rate of diff usion of solvent molecules is lower than the rate of polymer chain relaxation. If $n = 1$, the transport is non-Fickian mode, where chain relaxation is slower than the solvent penetration. If $0.5 < n > 1$, it indicates anomalous behaviour, where solvent penetration is much below the chain relaxation, while, in the case of $n <$ 0.5, it suggests less Fickian or pseudo-Fickian behaviour (Abraham et al., 2015; Wilson et al., 2012). As may be noted from the resultscollected in Table 3, the pure PS film has n value less than 0.5, and a graph Q_t vs. $T^{1/2}$ was plotted. It can be seen from the Fig. 4 that the molar uptake of water increases very rapidly in the PS because of its high hygroscopic nature, and is being reduced kinetically and quantitatively at the OS crosslinked samples (PS + OS), leading to a considerable sorption reduction due to an eff ective crosslinking of OS with the starch. It can also be observed that the swelling continues at a considerably fast rate, since the concentration gradient of penetrate solvent molecules is larger in the matrix. The least solvent absorption was recorded for PS + OS3/CNF5, which is due to the synergistic eff ect of the crosslinker, as well as well dispersed reinforcing filler CNFs in the suggesting that the mechanism is less Fickian (Balakrishnan et al.,2017). On the other hand, other crosslinked films have n values of nearly 0.5 which indicates Fickian behaviour, that might be due to the crosslinking that restricts the solvent penetration through the samples.

Table 3
WVTR and OTR of the films.

Sample	Thickness (mm)	WVTR (g $min^{-1} m^{-2}$)	OTR ($cm^3 m^{-2} d^{-1}$)
PS	0.32 ± 0.017	0.074 ± 0.015	29.44 ± 1.36
PS + OS1	0.24 ± 0.04	0.065 ± 0.090	21.07 ± 2.36
PS + OS1/CNF5	0.26 ± 0.035	0.060 ± 0.015	19.82 ± 1.68
PS + OS3	0.22 ± 0.016	0.043 ± 0.009	13.81 ± 3.56
PS + OS3/CNF5	0.27 ± 0.043	0.038 ± 0.007	10.27 ± 1.23

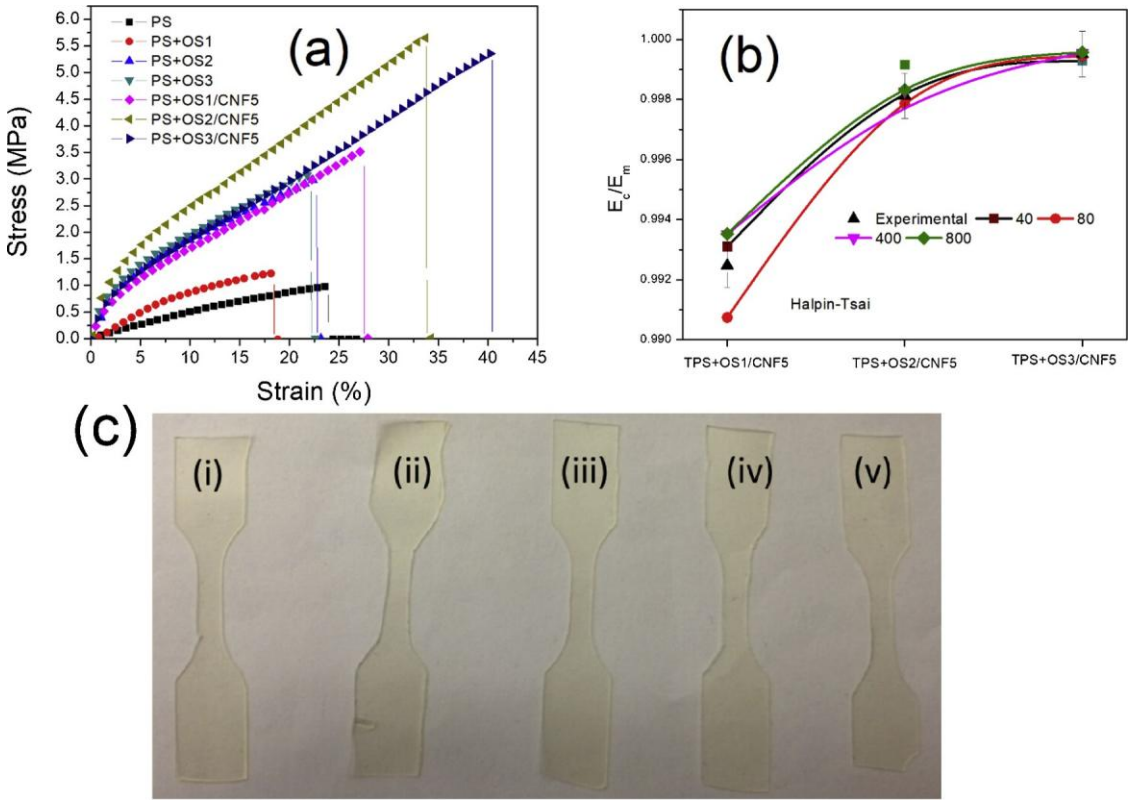

Fig. 5. (a) Stress-Strain curve of nanocomposites; (b) Theorotical prediction of tensile data (c) Images of samples (i) PS (ii) PS + OS1 (iii) PS + OS1/CNF5 (iv) PS + OS3 (v) PS + OS3/CNF5.

The Diff usion coeffi cient (D) is a kinetic parameter which indicates the rate of solvent diff usion into the system, which can be correlated with the segmental mobility of the polymer chains. The Diff usion coeffi cient can be calculated using the formula of Fickian law (Schurtenberger and Brown, 1996):

$$D = \left(\frac{h\theta}{4Q\infty}\right)^2 \qquad (11)$$

where h is the thickness of the sample and θ is the slope of linear portion of the sorption curve. The diff usivity of solvent is influenced strongly by the microstructure of the matrix, as well as the reinforcing phase, such as the pores that may form during the drying process. At a high level of reinforcement and crosslinking, the diff usion coeffi cient thus tends to decrease because of the decrease of matrix free volume. The permeation of a water into a film, however, depends on the diffusivity, as well as on the sorption. Permittivity and diff usivity of the films thus lowers with the CNFs concentration, which is due to the formation of a web-like structure.

The sorption (S) and permeability (P) coeffi cients of water at room temperature were also calculated (Table 2) using the following equations:

$$S = \frac{M_\infty}{M_0} \quad (12)$$

$$P = D \times S \quad (13)$$

where M∞ is the initial weight and M0 is the final weight of the sample. The Permeability coeffi cient (P) gives an overview of permeability of the films towards the solvent. Permeability coeffi cient of the nanocomposite films decreases with filler reinforcement which is due to the effective dispersion of CNF over the crosslink matrix and restricts the permeation of water molecules in between the sample where as in the case of crosslinked films, the permeability coefficient decreases due to the decrease in free volume within the matrix.

Swelling parameters give an idea about interfacial strength, crosslinking efficiency and degree of dispersion. The swelling coefficient is an index of ability with which the sample swells, and is calculated as follows:

$$\text{Swelling coefficient} = \left[\frac{(M_2 - M_1)}{M_1}\right] \times \text{density of solvent} \quad (14)$$

$$\text{Swelling I ndex} = \left[\frac{(M_2 - M_1)}{M_1}\right] \times 100 \quad (15)$$

where M_1 is the dry weight of the sample, and M_2 is the swollen weight of the sample. The values of both are found to decrease with increase of OS concentration and CNFs` dispersion, being related to the decrease of free volume within the matrix (Song et al., 2017).

3.6. Barrier properties

Shelf-life plays an important role in the packaging films and it de- pends mainly on the humidity and oxygen permeability through the packaging films. A humidity atmosphere with the presence of oxygen favours microbial growth, and gradually spoils the quality of food in- side (Malmir et al., 2017; Nair et al., 2017). Moreover, the reduced transmission rate favours increasing the degradation rate, since it de- pends on the transport of water from the surface to the bulk of the material (Park et al., 2003). In that respect, the water vapour trans- mission rate (WVTR) and oxygen transmission rate (OTR) measurements of the representative films were evaluated as the most important parameters for these properties (Wang et al., 2018). As seen from Table 3, both parameters decrease remarkably by the increasing of the content of OS, as well as CNFs, indicating high blocking of the hydrophilic hydroxyl groups, acting as a barrier that blocks the incoming water vapors, as well as the oxygen. The OTR is 29.44 $cm^3\ m^{-2} d^{-1}$ for the reference sample (neat PS) and 10.27 $cm^3\ m^{-2}\ d^{-1}$ for the cross-linked film with 3 wt.% OS and 5 wt.% CNFs. For the film prepared with the highest content of both components, compared to the reference film, the PS + OS3/CNF5

shows almost three-fold reduction in the OTR rate with respect to the neat sample. The results correlate with the formation of a dense structure over the crosslinked sample that reduces the transmission rates. The observed transmission rate is also much lower than that reported in the literature (Nair et al., 2017; Narayanan et al., 2017).

3.7. Mechanical properties

The effect of crosslinking and reinforcement by CNFs on the mechanical properties of starch films was evaluated by the tensile properties (tensile strength, and elongation at break), as shown in Fig. 5 by the stress-strain curve. A significant improvement in the tensile properties of PS upon the addition of crosslinkers (PS-OS1, PS-OS2, PS-OS3) and CNFs (PS-OS1/CNF5, PS-OS2/CNF5, PS-OS3/CNF5) was observed as compared to neat PS. The maximum tensile strength was recorded for the PS-OS2/CNF sample, which was due to the synergistic effect of both crosslinker and CNFS as reinforcing filler. A maximum five-fold improvement (from 0.950M Pa to 5.64M Pa) in tensile strength and twofold (from 24.75% to 40.43%) increment in the elongation was observed for neat PS with crosslinked and CNF contained films with maximum strength (Table 4). The increase in tensile properties is attributed primarily to the enhanced interfacial adhesion of matrix and CNFs, and good compatibility of starch with OS (Chang et al., 2004; Xu et al., 2015), resulting in chemical and physical interactions between the PS, OS and also CNFs. The crosslinked films are brittle and have less percentage of elongation due to the restricted chain mobility of the PS macromolecular chain (Angellier et al., 2006). On the other hand, the percent of elongation decreased for PS-OS3/CNF 5 compared to PSOS2/CNF 5. This may be due to an extreme stiffening effect of both crosslinker, as well as CNFs, on the starch. The improvement in the elongation may be due to a uniform distribution of CNFs over the matrix, leading to better load transfer characteristics from the CNFs to the matrix and the film to absorb and dissipate the energy better upon the application of external force (Saini et al., 2017). At higher loading of CNFs and crosslinker, a high degree of entanglement and crosslink may reduce the crystallinity and increase the amorphous phase that can also contribute to the percentage of elongation (Yue et al., 2013). In cellulose-based nanocomposites, the unusual reinforcement effect obtained by nano-sized elements is attributable to the formation of a rigid network of nanofibers connected by hydrogen bonds and also by mutual entanglements. Chung et al. (Chung et al., 2010) studied the effect of nanoclay on thermoplastic starch matrix. The tensile strength of composite upon 5 wt.% of nanoclay increases only by 30% compared toneat starch matrix. In that study the elongation at break decreases due to poor dispersion of clay platelets and ineffective stress transfer behavior. Fig. 5c. shows the images of crosslinked nanocomposite films.

Table 4
Tensile data of nanocomposites.

Sample code	Tensile strength (MPa)	Elongation (%)
PS	0.98 ± 0.04	23.71 ± 1.18
PS + OS1	1.24 ± 0.06	18.31 ± 0.91
PS + OS2	3.04 ± 0.15	22.65 ± 1.13
PS + OS3	3.11 ± 0.15	22.07 ± 1.10
PS + OS1/CNF 5	3.50 ± 0.17	27.36 ± 1.36
PS + OS2/CNF 5	5.63 ± 0.28	33.58 ± 1.67
PS + OS3/CNF 5	5.35 ± 0.26	40.18 ± 2.00

3.8. Theoretical prediction of mechanical data

In order to evaluate the reinforcing efficiency of cellulose nanofibers on the matrix, most common theoretical model Halpin-Tsai used to compared with experimental data (Lee et al., 2014; Faraz et al., 2014) (Fig. 5b). We choose Halpin-Tsai specifically due to its effectiveness in predicting the stiffness and modulus of composite reinforced with fibers and its adaptability to various filler loading and wide range of filler morphology like fiber, layer structure etc. Since the length of fiber is not easly to optimize due to its long interconnecting fiberous structure, we assume the length as 500 nm, 1 μm, 5 μm and 10 μm respectively and average diameter as 25 nm as reported by our previous study (Balakrishnan et al., 2017). So, the theoretical values are calculated considering four different aspect ratio (40,80,400,800 respectively). According to the theory,

$$\frac{E_c}{E_m} = \frac{1 + \omega\dfrac{\left(E_f/E_m\right)-1}{\left(E_f/E_m\right)+\omega}\varphi}{1 - \omega\dfrac{\left(E_f/E_m\right)-1}{\left(E_f/E_m\right)+\omega}\varphi} \tag{16}$$

Where, Ec, Em amd Ef are the modulus of composite, matrix and filler respectively. ω is the shape factor (2 l/d), φ is the volume fraction of filler. Since the filler was isolated from pineapple leaf, modulus of fiber calculated by the fillowing equation

$$Ef = \frac{(\omega + \varphi)E_c - \omega(1-\varphi)E_m}{\beta[(\omega\varphi + 1)E_m - (1-\varphi)E_c}E_m \tag{17}$$

For the fitting curve we can see that the composite fits well with higher aspect ratio, which in turn clarifies the improved barrier and mechanical properties of crosslinked nanocomposites. Due to the higher aspect ratio of prepared nanofiber, it can act as a barrier within the matrix that decreases the free volume with in the matrix and thereby improve the transport and barrier resistance. Also, due to high aspect ratio it can easily transfer the stress to the matrix and improve the elongation percentage.

3.9. Antibacterial properties

Antibacterial studies of crosslink nanocomposite were carried out in four bacteria strains *E. coli, S. typhimurium, St. aureus and B. cereus* (Table 5).

Samples with higher crosslinker content and nanoreinforcement found to be more resistant against bacterial pathogens. This may be primarily due to the blending of starch with plasticizer glycerol and crosslinker tetra aldehyde of sucrose (Mlalila et al., 2018). Priya et.al studied anti-bacterial eff ect of starch with PVA crosslinked with glutaraldehyde and found that both crosslinker and plasticizer citric acid induce antibacterial properties to the films (Priya et al., 2014). In this study, starch was crosslinked with oxidized sucrose which leads to the formation of acetal. The antimicrobial activity is primarily due to the following reasons; (1)acetal group can release cation charges ion which interacts with anionic charges of microbial cell membranes by electrostatic bonding. This specific interaction leads to increased cell permeability and leakage of intercellular components which finally leads to the cell death (Nicosia et al., 2015; Papineau et al., 1991) (2) Low permeability and hydrophobia of nanocomposite films that reduces the attraction of bacterial species (Zhang et al., 2012). From Table 5, we can confirm that PS-OS3 CNF 5 is most eff ective that of others that produced zones of inhibition against *Sstaphylococcus aureus, Escherichia coli, Salmonella typhimuriu and Bacillus*

Table 5
Antibacteial studies of prepared nanocomposite films against four bacterial strains.

Sample Code	Bacterial Strains	*MIC% W/V*
Control	*E. coli*	6.97 ± 0.63
	S. typhimurium	7.20 ± 0.29
	St. aureus	7.77 ± 0.41
	B. cereus	7.10 ± 0.35
PS + OS1	*E. coli*	3.70 ± 0.45
	S. typhimurium	4.07 ± 0.33
	St. aureus	4.4 ± 0.64
	B. cereus	4.1 ± 0.21
PS + OS2	*E. coli*	3.7 ± 0.37
	S. typhimurium	4.0 ± 0.54
	St. aureus	4.3 ± 0.61
	B. cereus	4.3 ± 0.44
PS + OS3	*E. coli*	3.7 ± 0.37
	S. typhimurium	4.0 ± 0.54
	St. aureus	4.3 ± 0.61
	B. cereus	4.3 ± 0.44
PS + OS1 CNF5	*E. coli*	3.8 ± 0.62
	S. typhimurium	4.2 ± 0.29
	St. aureus	4.1 ± 0.90
	B. cereus	4.3 ± 0.68
PS + OS2 CNF 5	*E. coli*	4.0 ± 0.61
	S. typhimurium	4.2 ± 0.28
	St. aureus	3.7 ± 0.60
	B. cereus	4.0 ± 0.49
PS + OS3 CNF 5	*E. coli*	4.3 ± 0.54
	S. typhimurium	4.3 ± 0.37
	St. aureus	3.7 ± 0.68
	B. cereus	4.1 ± 0.36

cereus.

4. Conclusions

Fully bio-based films were prepared by the solvent casting technique using glycerol plasticized corn starch, diff erent ratios of preoxidised sucrose (OS) as a crosslinker, and cellulose nanofibils (CNFs) as a reinforcing filler. The crosslinking effi ciency and compactability of components were confirmed by FTIR spectroscopy and SEM imaging, respectively, to be related to the chemical and physical interactions of hydroxyl groups of PS and CNFs with aldehydes. There is an improvement in functional (a decrease of water adsorption, diff usion, permeability and swelling) and barrier (reduction of water vapour transmission and oxygen permeability) performance

of films. Mechanical performance showed remarkable improvement after crosslinking and reinforcement. Crosslink nanocomposite exhibits resistance towards anti-bacterial pathogens. The prepared nanocomposite films can be an alternative to the existing ones in food packaging applications.

Acknowledgement

The authors are grateful to Department of Science and Technology (DST) for awarding an INSPIRE fellowship to Preetha Balakrishnan, DST Nanomission for instrumental facilities to IIUCNN and this study was financially supported by Project "Agropreparations of the new generation: a strategy of construction and realization" (Agreement No074-02-2018-328) in accordance with Resolution No 220 of the Government of the Russian Federation of April 9, 2010/

References

Abdel-Halim, E.S., Al-Deyab, S.S., 2014. Antimicrobial activity of silver/starch/poly- acrylamide nanocomposite. Int. J. Biol. Macromol. 68, 33–38. https://doi.org/10.1016/j.ijbiomac.2014.04.025.

Abraham, J., Maria, H.J., George, S.C., Kalarikkal, N., Thomas, S., Joseph, K., Thomas, S.,2015. Transport characteristics of organic solvents through carbon nanotube filled styrene butadiene rubber nanocomposites: the influence of rubber–filler interaction, the degree of reinforcement and morphology. Phys. Chem. Chem. Phys. 17,11217–11228. https://doi.org/10.1039/C5CP00719D.

Akrami, M., Ghasemi, I., Azizi, H., Karrabi, M., Seyedabadi, M., 2016. A new approach in compatibilization of the poly(lactic acid)/thermoplastic starch (PLA/TPS) blends.Carbohydr. Polym. 144, 254–262.

Angellier, H.élène, Molina-Boisseau, Sonia, Dole, Patrice, Dufresne, Alain, 2006.Thermoplastic Starch−Waxy Maize Starch Nanocrystals Nanocomposites. https://doi.org/10.1021/BM050797S.

Arun, S., Kumar, Ka A., Sreekala, M.S., 2012. Fully biodegradable potato starch compo- sites: eff ect of macro and nano fiber reinforcement on mechanical, thermal and water-sorption characteristics. Int. J. Plast. Technol. 16, 50–66. https://doi.org/10.1007/s12588-012-9026-4.

Assis, R.Q., Lopes, S.M., Costa, T.M.H., Flôres, S.H., Rios, A., de, O., 2017. Active bio- degradable cassava starch films incorporated lycopene nanocapsules. Ind. Crops Prod. 109, 818–827. https://doi.org/10.1016/J.INDCROP.2017.09.043.

Averous, L., Moro, L., Dole, P., Fringant, C., 2000. Properties of thermoplastic blends: starch-polycaprolactone. Polymer (Guildf.) 41, 4157–4167. https://doi.org/10.1016/ S0032-3861(99)00636-9.

Balakrishnan, P., Sreekala, M.S., Kunaver, M., Huskić, M., Thomas, S., 2017.

Morphology, transport characteristics and viscoelastic polymer chain confinement in nano- composites based on thermoplastic potato starch and cellulose nanofibers from pineapple leaf. Carbohydr. Polym. https://doi.org/10.1016/j.carbpol.2017.04.017.

Canisag, H., 2015. Bio-crosslinking of starch films with oxidized sucrose. Text. Merch. Fash. Des. Diss. Theses, Student Res. pp. 6.

Chang, Y.H., Lim, S.T., Yoo, B., 2004. Dynamic rheology of corn starch-sugar composites.J. Food Eng. 64, 521–527. https://doi.org/10.1016/j.jfoodeng.2003.08.017.

Chen, B., Dang, L., Zhang, X., Fang, W., Hou, M., Liu, T., Wang, Z., 2017. Physicochemical properties and micro-structural characteristics in starch from kudzu root as affected by cross-linking. Food Chem. 219, 93–101. https://doi.org/10.1016/j.foodchem.2016.09.128.

Chung, Y.L., Ansari, S., Estevez, L., Hayrapetyan, S., Giannelis, E.P., Lai, H.M., 2010. Preparation and properties of biodegradable starch-clay nanocomposites. Carbohydr. Polym. 79, 391–396. https://doi.org/10.1016/j.carbpol.2009.08.021.

Da Róz, a.L., Ferreira, a.M., Yamaji, F.M., Carvalho, a.J.F., 2012. Compatible blends of thermoplastic starch and hydrolyzed ethylene-vinyl acetate copolymers. Carbohydr. Polym. 90, 34–40. https://doi.org/10.1016/j.carbpol.2012.04.055.

Dang, K.M., Yoksan, R., 2016. Morphological characteristics and barrier properties of thermoplastic starch/chitosan blown film. Carbohydr. Polym. 150, 40–47. https://doi.org/10.1016/J.CARBPOL.2016.04.113.

Das, K., Ray, D., Bandyopadhyay, N.R., Sahoo, S., Mohanty, A.K., Misra, M., 2011. Physico-mechanical properties of the jute micro/nanofibril reinforced starch/poly-vinyl alcohol biocomposite films. Compos. Part B Eng. 42, 376–381. https://doi.org/10.1016/j.compositesb.2010.12.017.

Faraz, M.I., Besseling, N.A.M., Korobko, A.V., Picken, S.J., 2014. Structure–property re- lationships and modeling of the mechanical properties of a high-temperature resistant thermoset nanocomposite. Compos. Part B Eng. 56, 9–14. https://doi.org/10.1016/J.COMPOSITESB.2013.07.015.

Garcia, N.L., Ribba, L., Dufresne, A., Aranguren, M.I., Goyanes, S., 2009. Physico- Mechanical properties of biodegradable starch nanocomposites. Macromol. Mater.Eng. 294, 169–177. https://doi.org/10.1002/mame.200800271.

García, N.L., Ribba, L., Dufresne, A., Aranguren, M.I., Goyanes, S., 2009. Physico-me- chanical properties of biodegradable starch nanocomposites. Macromol. Mater. Eng.294, 169–177. https://doi.org/10.1002/mame.200800271.

Hietala, M., Mathew, A.P., Oksman, K., 2013. Bionanocomposites of thermoplastic starch and cellulose nanofibers manufactured using twin-screw extrusion. Eur. Polym. J. 49,950–956. https://doi.org/10.1016/j.eurpolymj.2012.10.016.

Hofreiter, B., Alexander, B., Wolff , I., 1955. Rapid estimation of dialdehyde content of periodate oxystarch through quantitative alkali consumption. Anal. Chem. John, M., Francis, B., Varughese, K., 2008. Effect of chemical modification on properties of hybrid fiber biocomposites. Compos. Part A Appl.

Karim, Z., Mathew, A.P., Grahn, M., Mouzon, J., Oksman, K., 2014.

Nanoporous mem- branes with cellulose nanocrystals as functional entity in chitosan: removal of dyes from water. Carbohydr. Polym. 112, 668–676. https://doi.org/10.1016/j.carbpol.2014.06.048.

Kaushik, A., Singh, M., Verma, G., 2010. Green nanocomposites based on thermoplastic starch and steam exploded cellulose nanofibrils from wheat straw. Carbohydr. Polym.82, 337–345. https://doi.org/10.1016/j.carbpol.2010.04.063.

Kim, H.-Y., Jane, J., Lamsal, B., 2017. Hydroxypropylation improves film properties of high amylose corn starch. Ind. Crops Prod. 95, 175–183. https://doi.org/10.1016/J.INDCROP.2016.10.025.

Kumirska, J., Czerwicka, M., Kaczyński, Z., Bychowska, A., Brzozowski, K., Thöming, J., Stepnowski, P., 2010. Application of spectroscopic methods for structural analysis of chitin and chitosan. Mar. Drugs 8, 1567–1636. https://doi.org/10.3390/md8051567.

Laskin, S., Sellakumar, A.R., Kuschner, M., Nelson, N., La Mendola, S., Rusch, G.M., Katz, G.V., Dulak, N.C., Albert, R.E., 1980. Inhalation carcinogenicity of epichlorohydrin in noninbred sprague-dawley rats23. JNCI J. Natl. Cancer Inst. 65, 751–757. https://doi.org/10.1093/jnci/65.4.751.

Lee, K.-Y., Aitomäki, Y., Berglund, La., Oksman, K., Bismarck, A., 2014. On the use of nanocellulose as reinforcement in polymer matrix composites. Compos. Sci. Technol.105, 15–27. https://doi.org/10.1016/j.compscitech.2014.08.032.

Li, M., Tian, X., Jin, R., Li, D., 2018. Preparation and characterization of nanocomposite films containing starch and cellulose nanofibers. Ind. Crops Prod. 123, 654–660. https://doi.org/10.1016/J.INDCROP.2018.07.043.

Liu, H., Xie, F., Yu, L., Chen, L., Li, L., 2009. Thermal processing of starch-based polymers. Prog. Polym. Sci. 34, 1348–1368. https://doi.org/10.1016/j.progpolymsci.2009.07.001.

Liu, D., Zhong, T., Chang, P.R., Li, K., Wu, Q., 2010. Starch composites reinforced by bamboo cellulosic crystals. Bioresour. Technol. 101, 2529–2536. https://doi.org/10.1016/j.biortech.2009.11.058.

Luchese, C.L., Spada, J.C., Tessaro, I.C., 2017. Starch content aff ects physicochemical properties of corn and cassava starch-based films. Ind. Crops Prod. 109, 619–626. https://doi.org/10.1016/J.INDCROP.2017.09.020.

Malmir, S., Montero, B., Rico, M., Barral, L., Bouza, R., 2017. Morphology, thermal and barrier properties of biodegradable films of poly (3-hydroxybutyrate-co-3-hydro- xyvalerate) containing cellulose nanocrystals. Compos. Part A Appl. Sci. Manuf. 93,41–48. https://doi.org/10.1016/j.compositesa.2016.11.011.

Mathew, A.P., Dufresne, A., 2002. Morphological investigation of nanocomposites from sorbitol plasticized starch and tunicin whiskers. Biomacromolecules 3, 609–617.https://doi.org/10.1021/bm0101769.

Matzinos, P., Tserki, V., Gianikouris, C., Pavlidou, E., Panayiotou, C., 2002. Processing and characterization of LDPE/starch/PCL blends. Eur. Polym. J. 38, 1713–1720.Mithra, A.K., Perlin, A.S., 1959. The reaction of sucrose with glycol-cleaving

oxidants1.Can. J. CI-IEMISTRY 37, 2047–2051.

Mittal, A., Garg, S., Kohli, D., Maiti, M., Jana, A.K., Bajpai, S., 2016. Eff ect of cross linking of PVA/starch and reinforcement of modified barley husk on the properties of composite films. Carbohydr. Polym. 151, 926–938. https://doi.org/10.1016/j.carbpol.2016.06.037.

Mlalila, N., Hilonga, A., Swai, H., Devlieghere, F., Ragaert, P., 2018. Antimicrobial packaging based on starch, poly(3-hydroxybutyrate) and poly(lactic-co-glycolide) materials and application challenges. Trends Food Sci. Technol. 74, 1–11. https://doi.org/10.1016/J.TIFS.2018.01.015.

Nair, S.B., Alummoottil, N.J., Moothandasserry, S.S., 2017. Chitosan-konjac gluco- mannan-cassava starch-nanosilver composite films with moisture resistant and antimicrobial properties for food-packaging applications. Starch – Stärke 69, 1600210.https://doi.org/10.1002/star.201600210.

Narayanan, M., Loganathan, S., Valapa, R.B., Thomas, S., Varghese, T.O., 2017. UV protective poly(lactic acid)/rosin films for sustainable packaging. Int. J. Biol. Macromol. 99, 37–45. https://doi.org/10.1016/j.ijbiomac.2017.01.152.

Neter, E., Westphal, O., Luderitz, O., Gorzynski, E.A., Eichenberger, E., 1956. Studies of enterobacterial lipopolysaccharides; eff ects of heat and chemicals on erythrocyte-modifying, antigenic, toxic and pyrogenic properties. J. Immunol. 76, 377–385.

Nicosia, A., Gieparda, W., Foksowicz-Flaczyk, J., Walentowska, J., Wesołek, D., Vazquez, B., Prodi, F., Belosi, F., 2015. Air filtration and antimicrobial capabilities of electrospun PLA/PHB containing ionic liquid. Sep. Purif. Technol. 154, 154–160. https://doi.org/10.1016/J.SEPPUR.2015.09.037.

Papineau, A.M., Hoover, D.G., Knorr, D., Farkas, D.F., 1991. Antimicrobial eff ect of wa- ter- soluble chitosans with high hydrostatic pressure. Food Biotechnol. 5, 45–57. https://doi.org/10.1080/08905439109549790.

Park, H.-M., Lee, W.-K., Park, C.-Y., Cho, W.-J., Ha, C.-S., 2003. Environmentally friendly polymer hybrids Part I mechanical, thermal, and barrier properties of thermoplastic starch/clay nanocomposites. J. Mater. Sci. 38, 909–915. https://doi.org/10.1023/A:1022308705231.

Prachayawarakorn, J., Sangnitidej, P., Boonpasith, P., 2010. Properties of thermoplastic rice starch composites reinforced by cotton fiber or low-density polyethylene. Carbohydr. Polym. 81, 425–433. https://doi.org/10.1016/j.carbpol.2010.02.041.

Priya, B., Gupta, V.K., Pathania, D., Singha, A.S., 2014. Synthesis, characterization and antibacterial activity of biodegradable starch/PVA composite films reinforced with cellulosic fibre. Carbohydr. Polym. 109, 171–179. https://doi.org/10.1016/j.carbpol.2014.03.044.

Reddy, N., Yang, Y., 2010. Citric acid cross-linking of starch films. Food Chem. 118, 702–711. https://doi.org/10.1016/J.FOODCHEM.2009.05.050.

Rico, M., Rodríguez-Llamazares, S., Barral, L., Bouza, R., Montero, B., 2016.

Processing and characterization of polyols plasticized-starch reinforced with microcrystallinecellulose. Carbohydr. Polym. 149, 83–93. https://doi.org/10.1016/J.CARBPOL.2016.04.087.

Saini, A., Yadav, C., Bera, M., Gupta, P., Maji, P.K., 2017. Maleic anhydride grafted linear low-density polyethylene/waste paper powder composites with superior mechanical behavior. J. Appl. Polym. Sci. 134, 45167. https://doi.org/10.1002/app.45167.

Saleesung, T., Saeoui, P., Sirisinha, C., 2017. Assessment of crosslink network and net- work defects of unfilled and filled ethylene-propylene-diene terpolymer using solid state nuclear magnetic relaxation spectroscopy. J. Appl. Polym. Sci. 134. https://doi. org/10.1002/app.44224.

Schurtenberger, P., Brown, W., 1996. Light Scattering: Principles and Development.American Chemical Societyhttps://doi.org/10.1021/jf201119v.

Song, K., Xu, H., Xie, K., Yang, Y., 2017. Keratin-based biocomposites reinforced and cross-linked with dual-functional cellulose nanocrystals. ACS Sustain. Chem. Eng. 5,5669–5678. https://doi.org/10.1021/acssuschemeng.7b00085.

Staroszczyk, H., Gottfried, K., Malinowska-Pańczyk, E., Kołodziejska, I., 2017. Clay-filled starch films. Part I: eff ect of clay kind and glycerol concentration on functional properties of composites. Starch – Stärke 69, 1500325. https://doi.org/10.1002/star.201500325.

Tang, X., Alavi, S., Herald, T.J., 2008. Eff ects of plasticizers on the structure and prop- erties of starch–clay nanocomposite films. Carbohydr. Polym. 74, 552–558. https://doi.org/10.1016/j.carbpol.2008.04.022.

Teacă, C.A., Bodîrlău, R., Spiridon, I., 2013. Eff ect of cellulose reinforcement on the properties of organic acid modified starch microparticles/plasticized starch biocomposite films. Carbohydr. Polym. 93, 307–315. https://doi.org/10.1016/j.carbpol.2012.10.020.

Veiga-Santos, P., Oliveira, L.M., Cereda, M.P., Scamparini, A.R.P., 2007. Sucrose and inverted sugar as plasticizer. Eff ect on cassava starch–gelatin film mechanical properties, hydrophilicity and water activity. Food Chem. 103, 255–262. https://doi.org/10.1016/J.FOODCHEM.2006.07.048.

Wang, G., Thompson, M.R., Liu, Q., 2012. Controlling the moisture absorption capacity in a fiber-reinforced thermoplastic starch using sodium trimetaphosphate. Ind. Crops Prod. 36, 299–303. https://doi.org/10.1016/j.indcrop.2011.10.015.

Wang, J., Gardner, D.J., Stark, N.M., Bousfield, D.W., Tajvidi, M., Cai, Z., 2018. Moisture and oxygen barrier properties of cellulose nanomaterial-based films. ACS Sustain. Chem. Eng. 6, 49–70. https://doi.org/10.1021/acssuschemeng.7b03523.

Wilson, R., George, S.M., Maria, H.J., Plivelic, S.S., A.K, Thomas, 2012. Clay intercalation and its influence on the morphology and transport properties of EVA/clay nanocomposites. Phys. Chem. C 20002–20014. https://doi.org/10.1021/jp302177y.

Xie, F., Flanagan, B.M., Li, M., Sangwan, P., Truss, R.W., Halley, P.J., Strounina, E.V., Whittaker, A.K., Gidley, M.J., Dean, K.M., Shamshina, J.L., Rogers,

R.D., McNally, T., 2014. Characteristics of starch-based films plasticised by glycerol and by the ionic liquid 1-ethyl-3-methylimidazolium acetate: a comparative study. Carbohydr. Polym.111, 841–848. https://doi.org/10.1016/J.CARBPOL.2014.05.058.

Xu, X., Yang, Y.Q., Xing, Y.Y., Yang, J.F., Wang, S.F., 2013. Properties of novel polyvinyl alcohol/cellulose nanocrystals/silver nanoparticles blend membranes. Carbohydr. Polym. 98, 1573–1577. https://doi.org/10.1016/j.carbpol.2013.07.065.

Xu, H., Canisag, H., Mu, B., Yang, Y., 2015. Robust and flexible films from 100% starch cross-linked by biobased disaccharide derivative. ACS Sustain. Chem. Eng. 3, 2631–2639. https://doi.org/10.1021/acssuschemeng.5b00353.

Xu, T., Jia, Z., Wang, S., Chen, Y., Luo, Y., Jia, D., Peng, Z., 2017. Self-crosslinkable epoxidized natural rubber–silica hybrids. J. Appl. Polym. Sci. 134. https://doi.org/10.1002/app.44605.

Yin, Y., Li, J., Liu, Y., Li, Z., 2005. Starch crosslinked with poly(vinyl alcohol) by boric acid. J. Appl. Polym. Sci. 96, 1394–1397. https://doi.org/10.1002/app.21569.

Yue, Y., Han, G., Wu, Q., 2013. Transitional properties of cotton fibers from cellulose I to cellulose II structure. BioResources 8, 6460–6471. https://doi.org/10.15376/biores.8.4.6460-6471.

Zhang, S.D., Zhang, Y.R., Wang, Y.Z., Wang, X.L., 2012. Eff ect of crosslink on properties of thermoplastics dialdehyde sweet potato starch. Adv. Mater. Res. 629, 391–395.https://doi.org/10.4028/www.scientific.net/AMR.629.391.

Zhang, L., Zhang, S., Dong, F., Cai, W., Shan, J., Zhang, X., Man, S., 2014. Antioxidant activity and in vitro digestibility of dialdehyde starches as influenced by their physical and structural properties. Food Chem. 149, 296–301. https://doi.org/10.1016/J.FOODCHEM.2013.10.126.

Zhang, C., Li, F., Li, J., Wang, L., Xie, Q., Xu, J., Chen, S., 2017. A new biodegradable composite with open cell by combining modified starch and plant fibers. Mater. Des.120, 222–229. https://doi.org/10.1016/J.MATDES.2017.02.027.

Zhou, L., Zhao, G., Jiang, W., 2016. Mechanical properties of biodegradable polylactide/poly(ether-block-amide)/thermoplastic starch blends: eff ect of the crosslinking of starch. J. Appl. Polym. Sci. 133. https://doi.org/10.1002/app.42297. n/a-n/a.